

# Kraft Lignin: From Pulping Waste to Bio-Based Dielectric Polymer for Organic Field-Effect Transistors

Rosarita D'Orsi, Cristian Vlad Irimia, Jeannette J. Lucejko, Bilge Kahraman, Yasin Kanbur, Cigdem Yumusak, Mateusz Bednorz, Francesco Babudri, Mihai Irimia-Vladu,\* and Alessandra Operamolla\*

Lignin is an abundant biopolymer deriving from industrial pulping processes of lignocellulosic biomass. Despite the huge amount of yearly produced lignin waste, it finds scarce application as a fine material and is usually destined to be combusted in thermochemical plants to feed, with low efficiency, other industrial processes. So far, the use of lignin in materials science is limited by the scarce knowledge of its molecular structure and properties, depending also on its isolation method. However, lignin represents an intriguing feedstock of organic material. Here, the structural and chemical-physical characteristics of two kraft lignins, L1 and L2, are analyzed. First, several molecular characterization techniques, such as attenuated total reflectance - Fourier transform infrared spectroscopy, elemental analyses, gel permeation chromatography, evolved gas analysis-mass spectrometry, UV-vis,  $^{31}\text{P}$ - and  $^{13}\text{C}$ - nuclear magnetic resonance spectroscopies are applied to get insights into their different structures and their degree of molecular degradation. Then, their efficient application as gate dielectric materials is demonstrated for organic field-effect transistors, finding the increased capacity of L1 with respect to L2 in triggering functional and efficient devices with both p-type and n-type organic semiconductor molecules.

technological transition toward a green economy,<sup>[1]</sup> detachment from fossil products, and a reduction of pollution and CO<sub>2</sub> emissions. Likewise, the emerging necessity of safe, nontoxic, and ecologically sustainable organic electronics and bio-electronics, in opposition to the less sustainable inorganic counterparts, requires the use of green functional materials.<sup>[2,3]</sup> In this work, we focus on lignin, an abundant biopolymer synthesized by plants. Lignin is rich in aromatic ring content<sup>[4]</sup> and derives from the radical polymerization of C<sub>6</sub>C<sub>3</sub> alcoholic monomers (i.e., phenyl propanoid structures such as *p*-coumaryl alcohol or H unit, coniferyl alcohol or G unit, and sinapyl alcohol or S unit, represented in **Figure 1**), which occur via an enzyme-initiated dehydrogenation.<sup>[5]</sup> Therefore, lignin possesses an amorphous structure, presenting different kinds of connections among monomers, mostly based on ether or carbon-carbon linkages.<sup>[6]</sup> Lignin is industrially isolated on the scale of kilotons per year as a waste of diverse pulping processes, aimed at cellulose isolation, such as the sulfite, kraft, and soda processes, with minor quantities of lignin waste delivered by the organosolv process.<sup>[7,8]</sup> A complete

## 1. Introduction


Unlocking the potential of bio-based polymers and their application in materials science is essential to enable a correct

trially isolated on the scale of kilotons per year as a waste of diverse pulping processes, aimed at cellulose isolation, such as the sulfite, kraft, and soda processes, with minor quantities of lignin waste delivered by the organosolv process.<sup>[7,8]</sup> A complete

R. D'Orsi, J. J. Lucejko, A. Operamolla  
Dipartimento di Chimica e Chimica Industriale  
Università di Pisa  
via Giuseppe Moruzzi 13, Pisa (PI) I-56124, Italy  
E-mail: alessandra.operamolla@unipi.it

C. V. Irimia, B. Kahraman, Y. Kanbur, C. Yumusak, M. Bednorz,  
M. Irimia-Vladu  
Linz Institute for Organic Solar Cells (LIOS)  
Physical Chemistry  
Johannes Kepler University Linz  
Altenberger Str. Nr. 69, Linz A-4040, Austria  
E-mail: mihai.irimia-vladu@jku.at

B. Kahraman  
Department of Material Science and Nanotechnology Engineering  
TOBB ETU University  
Söğütözü, Söğütözü Cd. No. 43, Çankaya/Ankara 06510, Turkey  
Y. Kanbur  
Department of Chemistry  
Karabük University  
Balıklarkayası Mevkii, Karabük 78050, Turkey  
F. Babudri  
Dipartimento di Chimica  
Università degli Studi di Bari Aldo Moro  
via Edoardo Orabona 4, Bari (BA) I-70126, Italy

 The ORCID identification number(s) for the author(s) of this article can be found under <https://doi.org/10.1002/adsu.202200285>.

© 2022 The Authors. Advanced Sustainable Systems published by Wiley-VCH GmbH. This is an open access article under the terms of the Creative Commons Attribution License, which permits use, distribution and reproduction in any medium, provided the original work is properly cited.

DOI: 10.1002/adsu.202200285

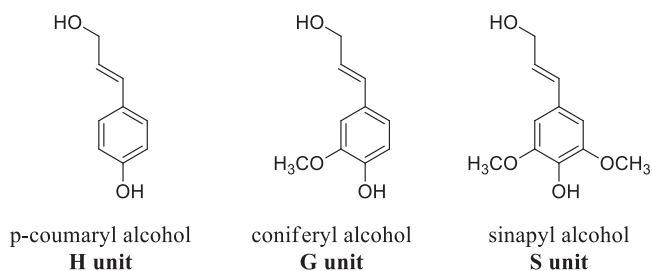


**Figure 1.** Phenyl propanoid structures of lignin alcoholic monomers.

biomass delignification often requires harsh thermochemical treatments which unavoidably cause lignin depolymerization and introduce new exogenous functional groups on the lignin molecular skeleton, like thiol groups in the case of kraft lignin and sulfonic or sulfonate groups in the case of lignosulfonates. Conversely, the advantage granted by these treatments consists in the solubilization of lignin, which is easily separated from the polysaccharide products and recovered. Despite the elevated amount of yearly produced lignin and its potential as carbon-based feedstock,<sup>[9]</sup> it is normally considered a low-value byproduct. Therefore, lignin main usefulness is often for combustion in biorefineries to feed industrial processes.<sup>[10]</sup>

Only recently, the idea of converting lignin into high added-value products and smart materials has been advanced.<sup>[11–13]</sup> So far, lignin has found application in sensing devices,<sup>[14–16]</sup> nanoparticles,<sup>[17–21]</sup> batteries and electrodes,<sup>[22–25]</sup> electrolyte membranes<sup>[26]</sup> and shape memory devices.<sup>[27–29]</sup> Recently, dielectric<sup>[30,31]</sup> and film forming<sup>[32]</sup> properties of lignin have been objects of attention, as well. However, most of the above-mentioned applications were achieved via lignin modification, such as further chemical manipulation or blends of lignin with other functional materials, such as polymers, nanoparticles, carbon nanotubes, etc. Demonstration of electronic properties and usefulness of lignin alone in electronic components is much harder, mainly because of the complexity introduced by differences in lignin structure and molecular properties, a consequence of diverse lignin sources and isolation methods. In connection with our research studies on green and bio-based alternative materials for organic electronics,<sup>[33–37]</sup> in this work we present kraft lignin application as gate dielectric in bottom-gate top-contacts organic field-effect transistor (OFET) devices.

We achieved characterization of two commercially available lignins, named lignin 1 (**L1**) and lignin 2 (**L2**), deriving from softwood by the kraft process. We describe their solubility, deposition conditions, and spectroscopic characterization, including information about lignin thermal stability. Differences in lignin structure, like the amount of polar or aromatic groups and fusion among monomers, are expected to produce an impact on the transistor performances.<sup>[38]</sup> This work represents a first investigation aimed at understanding how and to what extent the structural characteristics will affect lignin efficiency in serving as an excellent gate dielectric polymer for OFET devices.

## 2. Results and Discussion

### 2.1. Lignin Chemical Characterization

Results of analyses on the two lignins are collected in the **Table 1**. The two lignins derive from the same production process, with differences in the purification and isolation treatments. This introduces an important difference in lignin pH at 25 °C: 6.8 for **L1** and 10.0 for **L2** in water suspensions. **L2** lignin displayed 25.3% total ash content while a value of only 3.1% was found for **L1**. This pointed to significant degradation of **L2** during production. Qualitative elemental analysis of ashes from **L2** was performed by FE-SEM/EDS (field emission - scanning electron microscopy/energy dispersive X-ray spectroscopy) technique. Elemental composition of ashes revealed the presence of Na (20.7%), O (26.4%), S (4.13%) and K (3.20%) as main elements, suggesting the inorganic composition of the combustion residue, as will be confirmed by the evolved gas analysis shown later. Ashes composition suggested the use of NaOH during the isolation treatment. **L1** and **L2** structural and physical-chemical properties were different, including their solubility: while **L2** is dissolved in water, **L1** requires the presence of a basic solution for complete dissolution. Both lignins do not show good solubility in organic solvents (alcoholic solvents, ethyl acetate, tetrahydrofuran), except dimethylsulfoxide (DMSO). Complete dissolution of **L1** and **L2** was also achieved in 1:1 v:v mixtures of ethanol with 10% aqueous ammonia.

The elemental composition of the two lignins was corrected by the ash content. The formula weights (FW) extracted from

**Table 1.** Ash content, elemental analysis results, calculated empirical formulas, and formula weights, average molecular weights and polydispersities of **L1** and **L2**.

	Ash [%w/w]	pH	Elemental analysis [%w/w]					Empirical formula	FW [g mol <sup>-1</sup> ]	$M_n^a$ [Da]	$M_w^a$ [Da]	PI <sup>a</sup>	
			C	H	N	S	O <sup>b</sup>						OCH <sup>c</sup>
<b>L1</b>	3.1 <sup>d</sup>	6.8 <sup>e</sup>	61.00	6.27	0.65	1.51	27.47 <sup>f</sup>	1.16	C <sub>9</sub> H <sub>8.96</sub> O <sub>2.28</sub> S <sub>0.09</sub> N <sub>0.09</sub> (OCH <sub>3</sub> ) <sub>1.16</sub>	193.73	–	–	–
<b>L2</b>	25.3 <sup>d,g</sup>	10.0 <sup>h</sup>	46.57	5.19	0.07	1.68	21.17 <sup>f</sup>	0.70	C <sub>9</sub> H <sub>10.78</sub> O <sub>2.60</sub> S <sub>0.12</sub> N <sub>0.01</sub> (OCH <sub>3</sub> ) <sub>0.70</sub>	186.16	–	–	–
<b>Ac-L1</b>			62.20	5.73	0.25	0.76	31.06	1.16	C <sub>9</sub> H <sub>8.96</sub> O <sub>2.28</sub> S <sub>0.09</sub> N <sub>0.09</sub> (OCH <sub>3</sub> ) <sub>1.16</sub> (COCH <sub>3</sub> ) <sub>0.1</sub>	197.96	2150	4830	2.3
<b>Ac-L2</b>			58.38	5.34	0.39	1.22	34.67	0.70	C <sub>9</sub> H <sub>7.46</sub> O <sub>3.48</sub> S <sub>0.09</sub> N <sub>0.07</sub> (OCH <sub>3</sub> ) <sub>0.70</sub> (COCH <sub>3</sub> ) <sub>1.23</sub>	249.79	1260	3390	2.7

<sup>a</sup>)Values determined against polystyrene standards; <sup>b</sup>)The percentage of oxygen was calculated by the difference subtracting also the ash value; <sup>c</sup>)Based on C9 unit; <sup>d</sup>)Ash percentage was detected heating lignin at 525 °C (**L1**) or 600 °C (**L2**) in a muffle furnace until reaching a constant weight; <sup>e</sup>)Determined at 25 °C for a 5% w/w water suspension of **L1**; <sup>f</sup>)Oxygen percentage was also measured in a separate experiment, detecting 38.31% content for **L1** and 31.18% content for **L2**; <sup>g</sup>)Ashes from **L2** showed by SEM-EDS the following elemental composition: Na (20.7%), O (26.4%), S (4.13%), and K (3.20%); <sup>h</sup>)Determined at 25 °C for a 3% w/w water suspension of **L2**.

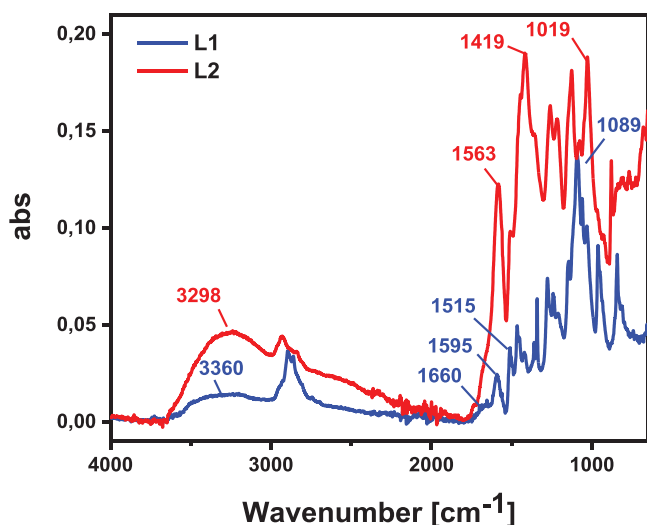


Figure 2. ATR-FTIR of L1 (blue line) and L2 (red line).

the elemental composition matched with the generic phenyl propanoid unit.<sup>[39]</sup> The moderate sulfur content found in both lignins is in line with the typical sulfur content of lignin originating from the kraft pulping process.<sup>[40]</sup> Elemental analyses on acetylated compounds Ac-L1 and Ac-L2 revealed a lower amount of acetyl groups per phenyl propanoid unit in Ac-L1, suggesting the presence of a higher number of monomeric fusions in the L1 structure than in L2, which, conversely, possesses a greater amount of free hydroxyl groups. This clearly pointed at a more depolymerized structure of L2 with respect to L1. Concerning average molecular weights, while Ac-L1 presents an  $M_n$  of 2150 Da and an  $M_w$  of 4830 Da, with a polydispersity index PI of 2.3, Ac-L2 presents an  $M_n$  of 1260 Da and an  $M_w$  of 3390 Da, with a polydispersity index PI of 2.7. These data suggest a slightly double degree of polymerization, based on the values of  $M_n$ /FW, of L1 with respect to L2 ( $\approx 10$  repeating units in L1 vs  $\approx 5$  in L2).

Attenuated total reflectance - Fourier transform infrared (ATR-FTIR) spectra are reported in blue and red lines for L1 and L2 in Figure 2. The spectral regions between 3800–2700  $\text{cm}^{-1}$  and 1850–700  $\text{cm}^{-1}$  include the most characteristic peaks of lignin.<sup>[42]</sup> These spectra are useful for a first evaluation of molecular properties. The two lignins were different for the C–O stretching signals: whilst L1 presents a high concentration of linear and aliphatic ethers, producing a signal at 1089  $\text{cm}^{-1}$ , L2 displays a much more pronounced peak at 1019  $\text{cm}^{-1}$ , that suggests a high content of aryl ethers. L2 presents an intense signal at 1563  $\text{cm}^{-1}$ , pointing at C=C stretching in aromatic systems or vinyl ethers with potential further delocalization. Vinyl structures in lignin can be the consequence of elimination processes from the lignin molecular backbone and are indicative of molecular degradation. Signals occurring in the range 1600–1700  $\text{cm}^{-1}$  in both spectra indicate the presence of carbonyl and further oxidized moieties.

The UV–vis normalized absorption profiles of the two lignins are reported in Figure 3. The absorption is produced by the aromatic rings contained in the lignin molecular skeleton. Spectra were acquired in dimethylsulfoxide, which allowed complete solubilization of the materials but limited the available

spectral window to a wavelengths range longer than 260 nm. UV–vis spectra were also acquired in 1:1 mixtures of ethanol:  $\text{NH}_4\text{OH}_{\text{aq}}$  10%. We used this solvent mixture to deposit lignin films. This investigation permitted us to evidence the capacity of hydroalcoholic ammonia to convert phenolic –OH of lignin into phenoxides in both materials. L1 and L2 display in DMSO absorption maxima at 286 and 280 nm, respectively, which can be attributed to noncondensed guaiacyl units.<sup>[42]</sup> Conjugated structures with aliphatic vinyl units or carbonyls produce further redshifted absorption maxima.<sup>[43]</sup> In DMSO, L1 presents a characteristic shoulder at  $\approx 340$  nm that can be assigned to more conjugated structures, such as  $\alpha$ -carbonyl groups and esters of hydrocinnamic acid.<sup>[44]</sup> L2 displays redshifted absorption up to 360 nm, confirming the presence of vinyl groups as found in stilbenes<sup>[45]</sup> or enol ethers,<sup>[46]</sup> formed during the kraft process by elimination reactions (for a comparison of L1 and L2 spectra in DMSO solution, see Figure S1, Supporting Information).

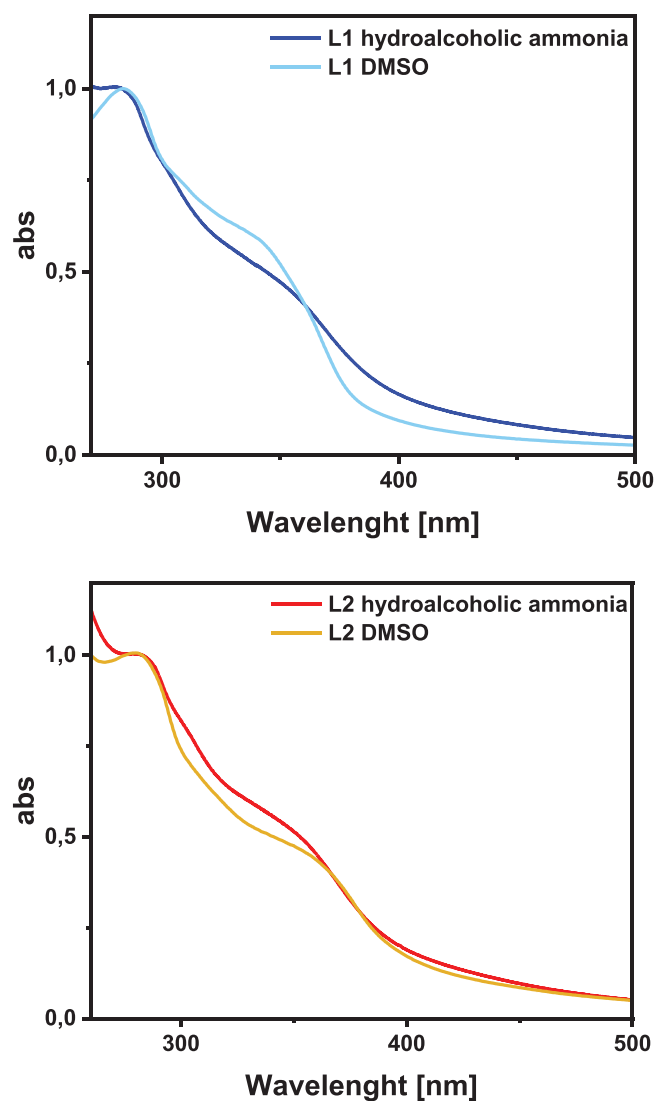
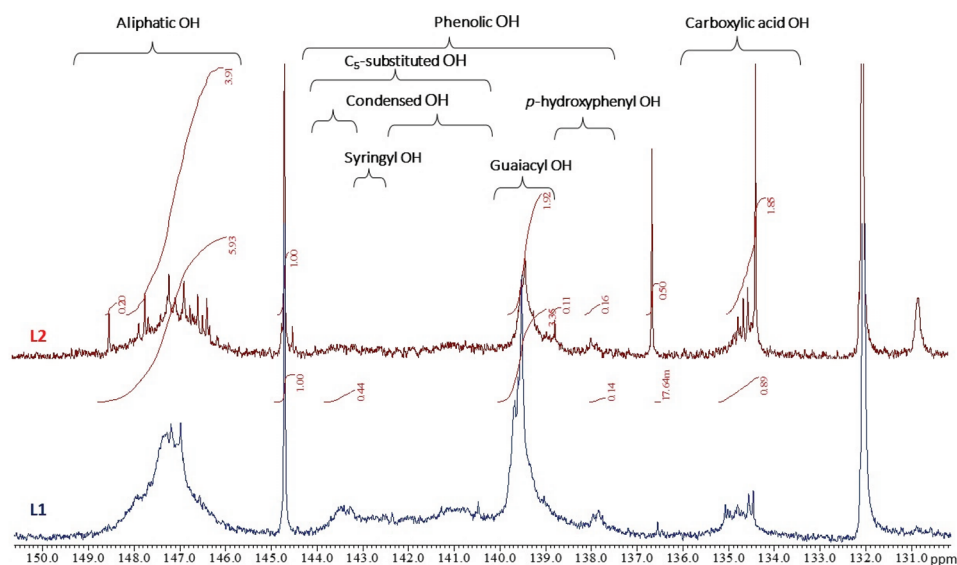


Figure 3. Normalized UV–vis absorption profiles of L1 (top panel) and L2 (bottom panel) at 0.5  $\text{mg mL}^{-1}$  concentration in DMSO and EtOH: $\text{NH}_4\text{OH}_{\text{aq}}$  1:1.



**Figure 4.**  $^{31}\text{P}$  NMR of L1 (bottom panel) and L2 (top panel). Integration is referred to as cholesterol used as an internal standard.

Therefore, the contemporary presence of aryl ethers and vinyl stretching bands in the L2 ATR-FTIR spectrum suggested the presence of aryl enol ethers in its structure. Switching to ethanol/ammonia solvent mixture, a shoulder at 353 nm appears in L1 absorption profile, indicating partial phenol deprotonation by aqueous ammonia. In L2 absorption profile this phenomenon appears as a band enhancement. Considering the pH of L2 water suspensions ( $\approx 10$ , vs a pH  $\approx 11$  of the hydroalcoholic ammonia), the smaller change was expectable.

Quantification of hydroxyl groups<sup>[48,49]</sup> and other functionalities by NMR spectroscopy was at this point necessary to predict the presence of negative charges in lignin films deposited from hydroalcoholic ammonia, and in particular, if the negative charges in the deposited lignin derive from phenoxides or other charged groups. This will be important, since ammonia is a weak base ( $pK_{a,\text{NH}_4^+} = 9.4$ ) and can only partially deprotonate the phenol groups of lignin ( $pK_a \approx 9-11$ ). Indeed, complete deprotonation of lignin phenol groups requires more alkaline environment.<sup>[44]</sup> The amount and typology of ionic charges will influence the lignin dielectric properties. Lignin derivatization of hydroxyls was necessary to enable quantitative studies based on  $^{31}\text{P}$ - and  $^{13}\text{C}$ -NMR. These reactions are shown in Scheme S1 in the Supporting Information.  $^{31}\text{P}$ -NMR spectroscopy can discriminate rapidly the typologies of lignin hydroxyl groups, aromatic and aliphatic, as well as condensed phenol units and carboxylic acid protons.<sup>[49]</sup> This technique represents

the most recognized method for hydroxyl groups quantification because it relies on the complete phosphorylation of OH-groups.<sup>[50]</sup> Figure 4 shows the results in the spectral range from 132 to 150 ppm. The calculated hydroxyl content is reported as  $\text{mmol g}^{-1}$  of lignin in Table 2. In both cases, the major phenolic contribution is due to the unit G. In L2, no signal related to C<sub>5</sub> substituted phenolic OH was found in the range from 140 to 143 ppm, revealing the absence of syringyl units. The signal found at 143.5 ppm was attributed to the carbon-carbon connection between the  $\beta$ -carbon of one unit and the C<sub>5</sub> of the phenolic unit ( $\beta$ -5 fusion).<sup>[51]</sup> Both lignins possess a higher amount of aliphatic than phenolic hydroxyls (1.98 vs 1.31  $\text{mmol g}^{-1}$  for L1 and 1.37 vs 0.73  $\text{mmol g}^{-1}$  for L2). L2 presents double amount of carboxylic acid groups (0.62  $\text{mmol g}^{-1}$  in L2 vs 0.30  $\text{mmol g}^{-1}$  in L1) and a significant presence of triclin, which is a type of flavonoid, a sign of L2 degradation.

$^{13}\text{C}$ -NMR spectroscopy of Ac-L1 and Ac-L2 provides a further detailed characterization especially on the typologies of aromatic carbons in both lignins. Results of the  $^{13}\text{C}$ -NMR analyses are reported in Table 3 in terms of the amount of aliphatic and aromatic hydroxyl groups detected as acetyl esters and of the number of carbon atoms bonded to  $-\text{OH}$  groups (aliphatic or aromatic) per phenyl propanoid unit ( $\text{C}_6\text{C}_3$ ).  $^{13}\text{C}$ -NMR analysis evidenced a higher content of primary aliphatic hydroxyls OH(I) in L1; conversely, secondary aliphatic hydroxyls OH(II) were more abundant in L2. Combining these results with the

**Table 2.** Hydroxyl content reported as  $\text{mmol per gram}$  of lignin, obtained by the integrated peaks of  $^{31}\text{P}$  NMR using cholesterol as internal standard. 1 g of lignin approximately corresponds to 5 mmol, based on the calculated empirical formula weights of Table 1.

	Aliphatic OH <sup>a,b)</sup>	OH( $\Phi$ ) <sup>c)</sup>	OH( $\Phi$ ) C5 substituted <sup>d)</sup>	$\beta$ -5 <sup>e)</sup>	G-OH <sup>f)</sup>	H-OH <sup>g)</sup>	COOH <sup>h)</sup>	Tricin <sup>i)</sup>
L1	1.98	1.31	0	0.15	1.12	0.05	0.30	0.01
L2	1.37	0.73	0	0	0.68	0.05	0.62	0.17

<sup>a)</sup>Integration limits; <sup>b)</sup>149.0–146.0 ppm; <sup>c)</sup>Total phenolic hydroxyl content, 144.0–137.4 ppm; <sup>d)</sup>Content of phenolic hydroxyls linked to the C5 carbon of the aromatic ring, 143.0–140.2 ppm; <sup>e)</sup>Content of link  $\beta$ -5, 143.5 ppm; <sup>f)</sup>Guaiacyl OH, 140.2–138.6 ppm; <sup>g)</sup>*p*-hydroxyphenyl OH, 138.8–137.4 ppm; <sup>h)</sup>136.0–133.6 ppm; <sup>i)</sup>137.0–136.0 ppm.



**Table 3.** Values calculated from  $^{13}\text{C}$  NMR of Ac-L1 and Ac-L2 and related to  $\text{C}_9$  unit.

	OH(I) <sup>a)</sup>	OH(II) <sup>b)</sup>	OH( $\Phi$ ) <sup>c)</sup>	OH(tot) <sup>d)</sup>	$\text{C}_{\text{Ar-O}}$ <sup>e)</sup>	$\text{C}_{\text{Ar-C}}$ <sup>f)</sup>	$\text{C}_{\text{Ar-H}}$ <sup>g)</sup>	Aliphatic C–O <sup>h)</sup>	$\text{OCH}_3$ <sup>i)</sup>
L1	0.35	0.15	0.49	0.99	0.56	0.75	1.04	0.93	0.59
L2	0.29	0.22	0.46	0.97	0.85	1.11	1.38	0.82	0.66

<sup>a)</sup>Integration limits: primary aliphatic hydroxyl groups, 171.2–169.9 ppm; <sup>b)</sup>Integration limits: secondary aliphatic hydroxyl groups, 169.9–169.4 ppm; <sup>c)</sup>Integration limits: phenolic groups, 169.2–167.2 ppm; <sup>d)</sup>Integration limits: total hydroxyl groups, 167.2–171.2; <sup>e)</sup>Integration limits: oxygenated aromatic carbons, 142–162 ppm; <sup>f)</sup>Integration limits: nonoxygenated aromatic carbons, 125–142 ppm; <sup>g)</sup>Integration limits: protonated aromatic carbons, 100–125 ppm; <sup>h)</sup>Integration limits: 58–90 ppm; <sup>i)</sup>Integration limits: 54–58 ppm.

higher aliphatic C–O content recorded in **L1**, confirmed the major presence of aliphatic ethers and alcohols in this lignin sample. Conversely, **L2** displayed 0.85 content of aromatic carbons linked to oxygen  $\text{C}_{\text{Ar-O}}$  vs 0.56 in **L1**. This pointed again to the abundance of aryl enol ethers in **L2**. This finding was confirmed by the higher integration values of aromatic carbons  $\text{C}_{\text{Ar-O}}$  and  $\text{C}_{\text{Ar-H}}$ , found in the range from 100 to 140 ppm, overlapping vinyl carbon signals. Apparently, **L1** displayed a less linear structure than **L2**, presenting the lowest content of  $\text{C}_{\text{Ar-H}}$ , 1.04 vs 1.38 of **L2**. Heteronuclear single quantum coherence (HSQC) bidimensional spectra of **L1** and **L2** showed typical signals of kraft lignin.<sup>[53]</sup> These spectra are reported in Figure S6 in the Supporting Information. The poorly populated region of  $\text{C}_{\text{Ar-H}}$  signals in **L2** was a further confirmation of ring condensation in this lignin. HSQC spectra also revealed the major relative occurrence of  $\beta$ -5,  $\alpha$ -O-4 fusions ( $\delta_{\text{C}}$  54.5 ppm,  $\delta_{\text{H}}$  3.10 ppm), corresponding to cyclic cumarane structures, in **L1**.

Evolved gas analysis - mass spectrometry (EGA-MS) analysis was applied to investigate the differences in thermal stability of **L1** and **L2**. EGA-MS can highlight structural alterations that occurred in lignin, such as side chain shortening, oxidation, or demethylation processes,<sup>[53–55]</sup> and furnish relevant information on lignin structure. The total ion thermograms (TITs), corresponding to the volatile products evolved in the temperature range of 50–700 °C for **L1** and **L2** (Figure 5, top panel) showed thermal degradation between 150 °C (5 min) and 300 °C (20 min). Despite the same quantity of sample was used for each analysis (200  $\mu\text{g}$ ), the relative abundance of evolved gases from **L1** and **L2** reflected the important difference in ash content between the two lignins. In EGA profiles the maxima of evolved gases were found at 246 °C for **L1** and 240 °C for **L2**. A shoulder after 15 min (260 °C) for **L2** was observed, while above 300 °C, a residue was registered only for **L1**. These differences are generally related to the strength of the intrapolymeric interactions of lignin which require different amounts of thermal energy to break and release the thermal degradation products.<sup>[56]</sup> Overall, **L2** is less resistant to degradation than **L1**, most likely due to the greater degree of structural alteration of **L2** concerning native lignin structure. The overall mass spectra of **L1** and **L2** were extracted from the thermal degradation zone, between 5 and 25 min, to highlight the contribution to degradation peaks of the produced fragment ions. These spectra are shown in the Supporting Information. The spectra were rich in fragments deriving from guaiacyl units.<sup>[57]</sup> **L1** presented fragments ( $m/z$  239 and 285) characteristic of the dehydroabietic acid, one of the main components of conifer resins, allowing to identify pine as the wood species used in the kraft process. **L2** displayed instead fragments formed from

retene ( $m/z$  219 and 234), a degradation product of dehydroabietic acid. Being derived from softwood (pine), therefore **L1** and **L2** contain only the monomers H and G displayed in Figure 1. The single-ion thermograms of relevant products released during EGA-MS analysis of **L1** and **L2** are shown in the bottom panels of Figure 4. These data confirm the significant differences existing between **L1** and **L2**. Primary pyrolysis fragments of vanillin and coniferyl alcohol, such as the  $m/z$  137 fragment, were more abundant in **L1** than in **L2**. **L1** displayed as well a more important evolution of vinyl guaiacol ( $m/z$  150), eugenol ( $m/z$  164), and dimers (G-G dimer stilbene-type,  $m/z$  272). The presence of evolved dimers in **L1**, absent in **L2**, confirmed the extensive phenomenon of depolymerization of **L2**. The higher abundance of secondary pyrolysis products in **L2**, such as fragment ions deriving from guaiacol ( $m/z$  124), alkylphenols ( $m/z$  107), and alkylbenzenes ( $m/z$  91), could be taken as a further indication of its structural degradation, as guaiacol is the smallest molecule representative of guaiacyl-lignin. These fragments are produced by pyrolysis reactions involving demethylation and demethoxylation of guaiacyl units. The relative abundance of the peak of *p*-formylguaiacol ( $m/z$  151) was relevantly higher in **L1** (confirmed by the overall mass spectra reported in the Supporting Information) pointing to a higher presence of oxidized moieties in **L1**.

Thanks to the extensive molecular structure characterization performed on **L1** and **L2**, we could sketch their chemical structures, as qualitatively represented in the Figure 6. Although the schematic representation roughly respects the stoichiometry deriving from NMR analysis, it evidences the major occurrence of enol ethers (green) and carboxylic groups (red) in **L2**.

## 2.2. Lignin Dielectric Spectroscopy

To understand potentialities of application of **L1** and **L2** as gate materials for organic field effect transistors, dielectric spectroscopy investigations were carried out in a metal–insulator–metal (MIM) structure with **L1** and **L2** lignin layers sandwiched between 1 mm wide, 80 nm thick bottom and top aluminum electrodes in cross geometry deposition. Lignins were easily deposited by doctor blading from a 100 mg mL<sup>-1</sup> solution in ethanol: 10% aqueous ammonia in volumetric ratio 1:1. The dielectric spectroscopy data for the two-lignin materials is presented in Figure 7. **L1** lignin (Figure 7a) shows a much more uniform dielectric behavior than **L2** (Figure 7b). This can be seen through a relatively constant capacitance value over the entire frequency range and, more importantly for a dielectric behavior in OFETs, through low losses with maximum value

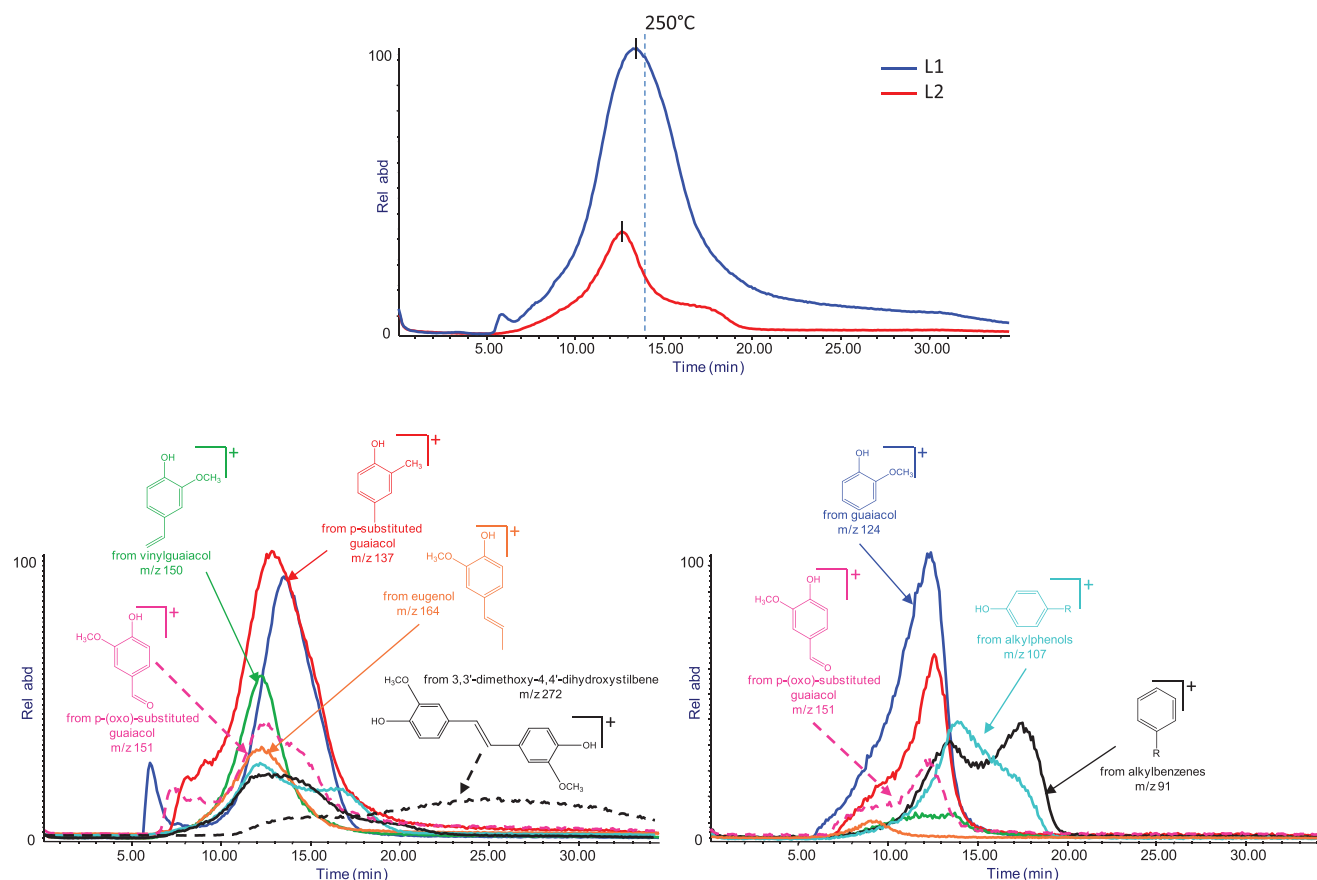


**Figure 5.** Top panel: Total ion thermograms (TITs) recorded by EGA-MS analysis for L1 and L2, where the maxima of evolved gases versus temperature were 246 and 240 °C for L1 and L2, respectively. Extracted ion thermogram of evolved gases during thermal degradation of L1 (bottom left panel) and L2 (bottom right panel). Fragment ions are shown in different colors:  $m/z$  91 (alkylbenzenes, black line), 107 (alkylphenols, light blue line), 124 (guaiacol, blue line), 137 (*p*-substituted guaiacol, red line), 150 (vinyl guaiacol, green line), 151 (*p*-formylguaiacol, magenta dashed line), 164 (eugenol, orange line), and 272 (stilbenes, black dashed line).

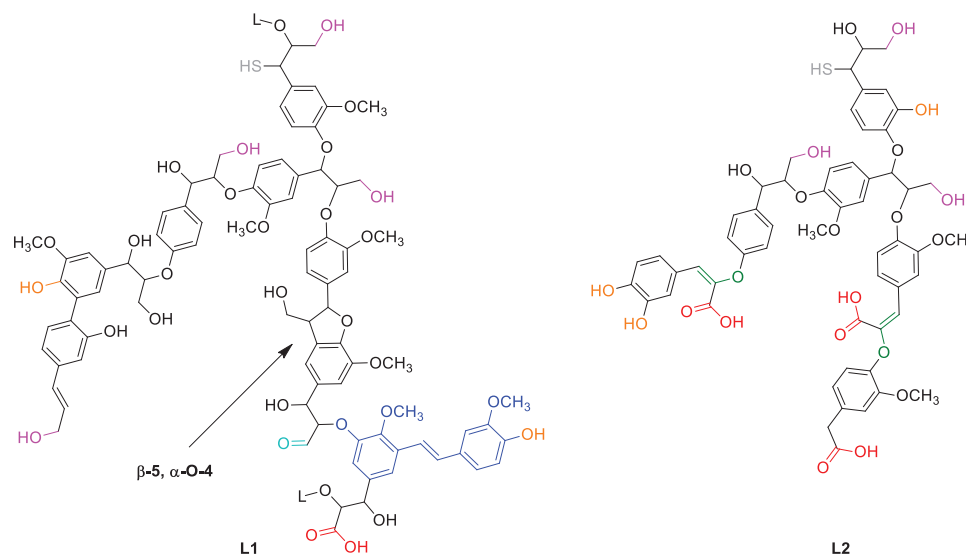


**Figure 6.** Schematic representation of L1 and L2 chemical structures, with indication of the most occurring chemical functionalities. The characteristic ( $\beta$ -5,  $\alpha$ -O-4) fusion, detected by HSQC, is highlighted by the arrow. Other chemical functionalities are highlighted in different colors: thiol groups introduced by the kraft process in gray, primary aliphatic alcohols in magenta, carbonyls in light blue, phenol groups in orange, carboxylic groups in red, enol ethers in green, stilbenes in dark blue.

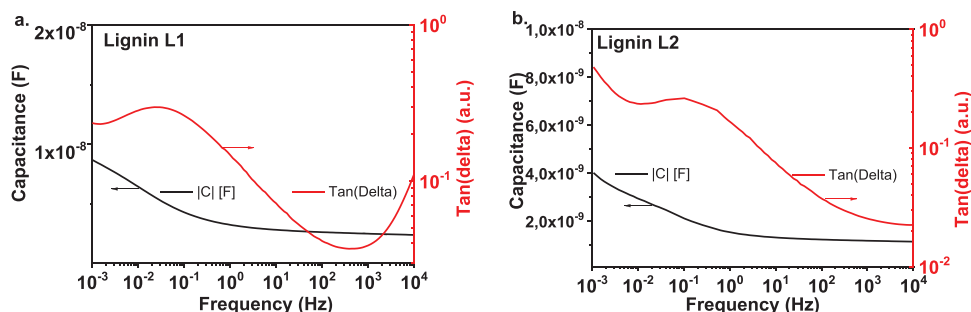


**Figure 7.** Dielectric spectroscopy in frequency range from 10 kHz to 1 MHz of a) L1 and b) L2 lignin.

of 0.25 even at 1 MHz frequency (i.e., red line in Figure 7a). Moreover, the loss angle curve shows relaxation in a frequency window that is irrelevant for fast electric sweeping measurements of the OFETs (i.e., the dome shape of the red curve in panel (a) of the Figure 7). The overall behavior of the L1 lignin is of a very good dielectric candidate for OFETs fabrication. In

comparison, the L2 lignin also shows a good dielectric behavior, with low losses and a relatively flat capacitance over a wide frequency range (Figure 7b). The maximum losses of lignin L2 are 0.5 at 1 MHz, and the relaxation (dome shape in tangent delta) occurs at a frequency range that is not important for fast electronic measurement, albeit the respective maximum occurs at a frequency of 0.1 Hz, that is higher than the respective value of L1, i.e., 0.02 Hz. The appearance of the relaxation mechanisms in both lignins implies that ionic species are present in the solid films, as expected for a deposition from aqueous ammonia, producing phenoxide and carboxylate anions. The concentration of  $-\text{COO}^-$  groups will be higher in L2, on the basis of what was observed from  $^{31}\text{P}$ -NMR spectroscopy. Since charges are apparently slightly more mobile in the case of L2, this can be explained by the presence of an approximately doubled concentration of carboxylate anions in L2 (0.62 mmol  $\text{g}^{-1}$  of L2, as reported in Table 2). This is reasonable, considering that phenol units will not be completely deprotonated in the hydroalcoholic ammonia. As will be seen in the section dealing with OFET devices fabrication and measurement, the presence of mobile charges in L2 lignin will have a significant impact on the behavior of devices. In addition, we observed an increased tendency for the L2 dielectric films to absorb water vapors, a fact that is not desired in case of OFET devices since the water vapors make the incorporated ions more mobile and give rise to hysteresis effects, and low drain–source currents.<sup>[59]</sup> With this respect, the films of L2 had to be scrupulously dried in vacuum overnight at temperature of 100 °C in order to reduce at minimum the influence of water in the dielectric layer. We performed dielectric measurements on cast films of L1 and L2 lignins in order to retrieve information about the specific dielectric constant of the two materials. With this respect we measured dielectric constants of  $6.3 \pm 0.9$  for L1, but we could not confidently determine the dielectric constant of L2 lignin dielectric because of the hygroscopic instability of the material.

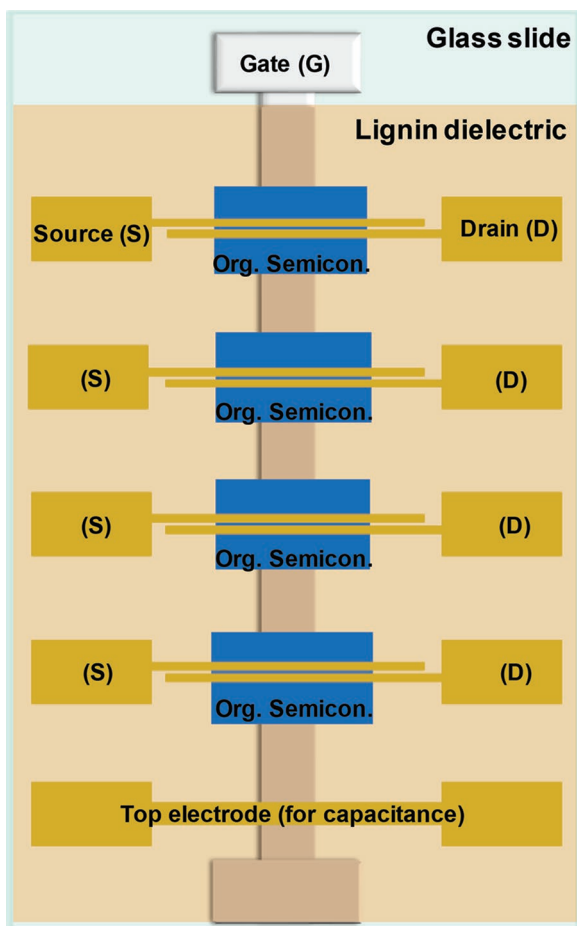


**Figure 8.** Schematic of the mask design employed for transistors fabrication. The gate electrode (G) was always aluminum, the source (S) and drain (D) electrodes were gold for pentacene semiconductor and aluminum for fullerene  $\text{C}_{60}$  based OFETs. The mask design allows us to measure the capacitance of the dielectric layer to be used for mobility calculation, via a metal–insulator–metal structure developed directly on top of the dielectric layer.

### 2.3. Lignin Dielectric Layers in OFETs

OFETs with L1 and L2 lignin were fabricated in staggered bottom-gate top-contact geometry, through a procedure amply described in the experimental section and in our previous publications.<sup>[59,60]</sup> A schematic of such geometry, including the OFET layers is displayed in Figure 8.

We investigated two possible dielectric choices for OFETs in this work: an inorganic–organic bilayer dielectric of

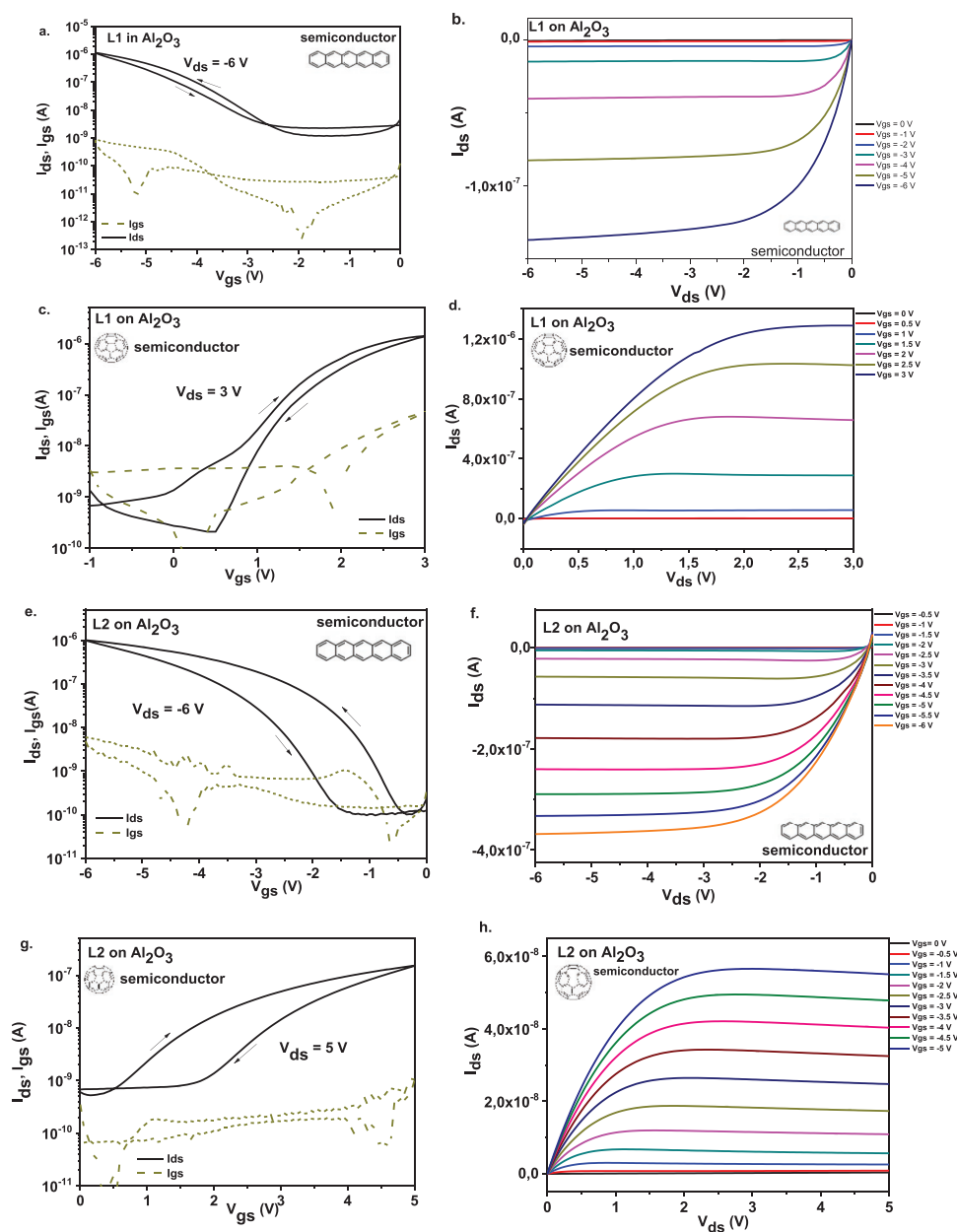


**Figure 9.** Transfer and output characteristic of spin coated lignins. Left panels (a)–(d) are referred to **L1** and right panel (e)–(h) to **L2**. a,b) **L1** on alumina dielectric and pentacene semiconductor. Specific capacitance of the dielectric,  $146.25 \text{ nF cm}^{-2}$ ; field effect mobility,  $2 \times 10^{-2} \text{ cm}^2 \text{ V}^{-1} \text{ s}^{-1}$ . c,d) **L1** on alumina dielectric and fullerene  $\text{C}_{60}$  semiconductor. Specific capacitance of the dielectric,  $146.25 \text{ nF cm}^{-2}$ ; field effect mobility,  $7 \times 10^{-2} \text{ cm}^2 \text{ V}^{-1} \text{ s}^{-1}$ . e,f) **L2** doctor bladed on alumina dielectric and pentacene semiconductor. Dielectric specific capacitance,  $48.9 \text{ nF cm}^{-2}$ ; field effect mobility,  $7 \times 10^{-3} \text{ cm}^2 \text{ V}^{-1} \text{ s}^{-1}$ . g,h) **L2** doctor bladed on alumina dielectric and fullerene  $\text{C}_{60}$  semiconductor. Specific capacitance,  $48.9 \text{ nF cm}^{-2}$ ; field effect mobility,  $8 \times 10^{-3} \text{ cm}^2 \text{ V}^{-1} \text{ s}^{-1}$ .

alumina and lignin (**L1** or **L2**) and a stand-alone lignin dielectric without alumina. The reason for needing to use of a capping layer for alumina in the form of an organic dielectric (lignin in this case) was detailed in our previous publications.<sup>[60,61]</sup> The **Figure 9** presents the transistor characteristics of pentacene and fullerene ( $\text{C}_{60}$ ) semiconductors deposited on combined inorganic–organic (alumina–lignin) dielectric. Between the two investigated lignin formulations, the **L1** displays more robust dielectric and interface properties. This is observable through a much more reduced hysteresis (see **Figure 9**, panels (a) and

(c) compared to respective transfer curves displayed in panels (e) and (g)). Moreover, the field effect mobility recorded for **L1** interface with the two semiconductors is significantly higher (factor of 3 for pentacene, and factor of 9 for  $\text{C}_{60}$ ) than in the respective case of **L2**. The specific capacitance of the **L2** is also a factor of 3 lower ( $49 \text{ nF cm}^{-2}$  vs  $146 \text{ nF cm}^{-2}$ ) compared to **L1** for films deposited from stock solutions of same concentration. The reason behind it might be the higher viscosity of the **L2** solution that produces films of higher thicknesses or its considerably lower purity. According to the compositional analyses



performed on **L2**, the higher inorganic ashes content (25.3%) represents a non-negligible contamination. On the other side, parallel attempts of removing ashes by solvent fractionation were sidled by an undesirable solvent chemical derivatization of **L2**.<sup>[62]</sup> We proceeded to the completion of the final comparison, namely fabrication of OFET devices with the two lignins as stand-alone dielectrics, and assessed both **L1** and **L2** lignin on plain aluminum gate electrodes, without the presence of alumina layer. We evaluated **L1** and **L2** lignin dielectric layers of various thicknesses, stemming from stock solution of various concentrations of the two lignins in 1:1 mixture of ethanol and ammonia. Nevertheless, we fabricated devices with satisfying performances from both **L1** and **L2** stand-alone dielectrics when  $C_{60}$  was used as semiconductor layer, but, when interfaced with pentacene semiconductor, only **L1** provided convincing results, as **Figure 10** demonstrates.

**L1**, used as stand-alone dielectric or on top of alumina interlayer, generated OFET devices with transfer characteristics having minimal hysteresis for both electron and hole channels. Nevertheless, the higher compactness (and possibly better interface) of alumina containing devices, shown in **Figure 9**, resulted in higher  $I_{ds}$  currents and inherently higher field effect mobilities. Both device parameters improved by an order of magnitude for the device containing alumina interfaced to **L1** compared to **L1** as stand-alone dielectric. When **L2** lignin was used as stand-alone dielectric and interfaced with  $C_{60}$ , the devices displayed similar drain currents and field effect mobilities to the ones recorded in the presence of alumina (**Figures 9g,h** and **10e,f**).

In the case of pentacene, the field effect mobility of the OFETs with stand-alone **L2** dielectric is clearly much lower than the respective results for stand-alone **L1** (see **Figure 10**, panels **(g)–(h)**). Indeed, when deposited on **L2** stand-alone dielectric, the field effect mobility measured is more than 1 order of magnitude lower than the respective value recorded on **L1** (i.e.,  $3.2 \times 10^{-4} \text{ cm}^2 \text{ V}^{-1} \text{ s}^{-1}$  vs  $4 \times 10^{-3} \text{ cm}^2 \text{ V}^{-1} \text{ s}^{-1}$ ). Likewise, the OFET field-effect mobility of pentacene was significantly lower (i.e., factor of 3) on **L2** when alumina was used as dielectric interlayer (**Figure 9**). For pentacene the molecular orientation is one of the requisites for inducing large aggregates.<sup>[62]</sup> However, it is well known that this semiconductor can yield polymorphic films upon evaporation.<sup>[63]</sup> This intricate behavior will probably require further studies to understand the limited aggregation capacity of pentacene on the two lignins, and the careful growth of pentacene monolayers will definitely shed more light into this aggregation mechanism.

Trying to elucidate the differences found in OFET characteristics and in the two semiconductors behavior, we investigated the film surface morphology of the two lignins, as well as the morphology of  $C_{60}$  and pentacene, grown by vacuum sublimation. Atomic force microscopy (AFM) topographies of **L1** and **L2** films (**Figures 11**, panels **(a)** and **(d)**) reveal similar, featureless and smooth surfaces, displaying root-mean-square (rms) roughness values of 5.4 nm for **L1** and 2.8 nm for **L2**, respectively. The surface roughness seemed ideal for the growth of organic semiconductors on top of them. Indeed, the AFM investigations of pentacene and  $C_{60}$  reveal a similar growth model of the two semiconductors on each of the two lignins, with featureless morphology of  $C_{60}$  and small grains in nanometer

size range for pentacene (see **Figure 11**, panels **(b)–(e)** and **(c)–(f)**, respectively). The good performances of  $C_{60}$  OFETs, recorded especially with **L1** gate dielectric layer were probably generated by an efficient self-organization of this semiconductor on lignin surface: this could be explained invoking favorable interactions between fullerene cages and lignin aromatic groups at the interface by  $\pi$ – $\pi$  stacking mechanism. Nevertheless,  $C_{60}$  does not yield similar OFET results when evaporated on stand-alone **L1** and **L2** lignins, used as gate dielectric. In these devices, fullerene displays comparable mobility values, but a significantly larger hysteresis when coupled **L2** dielectric (**Figures 10**). This points out at the presence of some trapping mechanism at the interface between the dielectric and semiconductor, raising from the intrinsic composition of **L2** and not from the morphology of fullerene.

The chemical structure and composition of **L2** (**Figure 6** and **Table 1**) plays a crucial role here, suggesting an increased tendency to entrap charges from this lignin. In the case of holes, this is consistent with the higher carboxylate groups content in **L2** deposited films. It is also important to note that the direction of the hysteresis occurrence (clockwise for the  $C_{60}$  and counter-clockwise for pentacene) indicates that the mobile ionic impurities in **L1** and **L2** lignins are not responsible for hysteresis occurrence: that is rather generated by the trapping at the interface of the two dielectric materials with the organic semiconductors,<sup>[59]</sup> and this trapping is more prominent in the case of **L2** lignin, especially when holes are the transported charges. At this point we think that the high ashes content of **L2** lignin is the main reason for these trapping events to occur, especially since the ashes contain oxides. Definitely, further studies are necessary to elucidate this behavior.

### 3. Conclusion

In this work, we achieved for the first time a correlation between the chemical structure of two kraft lignins and their performances as dielectric layers in organic field-effect transistors in the bottom-gate top-contacts device configuration. We thoroughly compared the chemical structures of **L1** and **L2** by using various investigation techniques. We pointed out the more degraded and depolymerized structure of **L2**, which showed a higher concentration of phenyl enol ethers and carboxyl groups and a higher content of ashes. When introduced as dielectric films into an OFET device, **L1** showed the best performance, with lower hysteresis and higher charge carrier mobilities for both semiconductors. This could be justified by two factors: a better interface of the **L1** lignin with both pentacene and  $C_{60}$  semiconductors; and the hypothesized trap effect exerted on charges by the carboxylate ions present on the **L2** skeleton at a higher extent. Furthermore, the lower purity of **L2**, demonstrated by 25.3% ashes content, can influence its dielectric properties in a major way. The presence of alumina gate interlayer is favorable in creating a denser dielectric layer that leads to generation of one order of magnitude higher drain currents and inherently one order of magnitude higher field effect mobilities for **L1**. Nevertheless, **L1** lignin can be employed as stand-alone dielectric too, with good performance for low

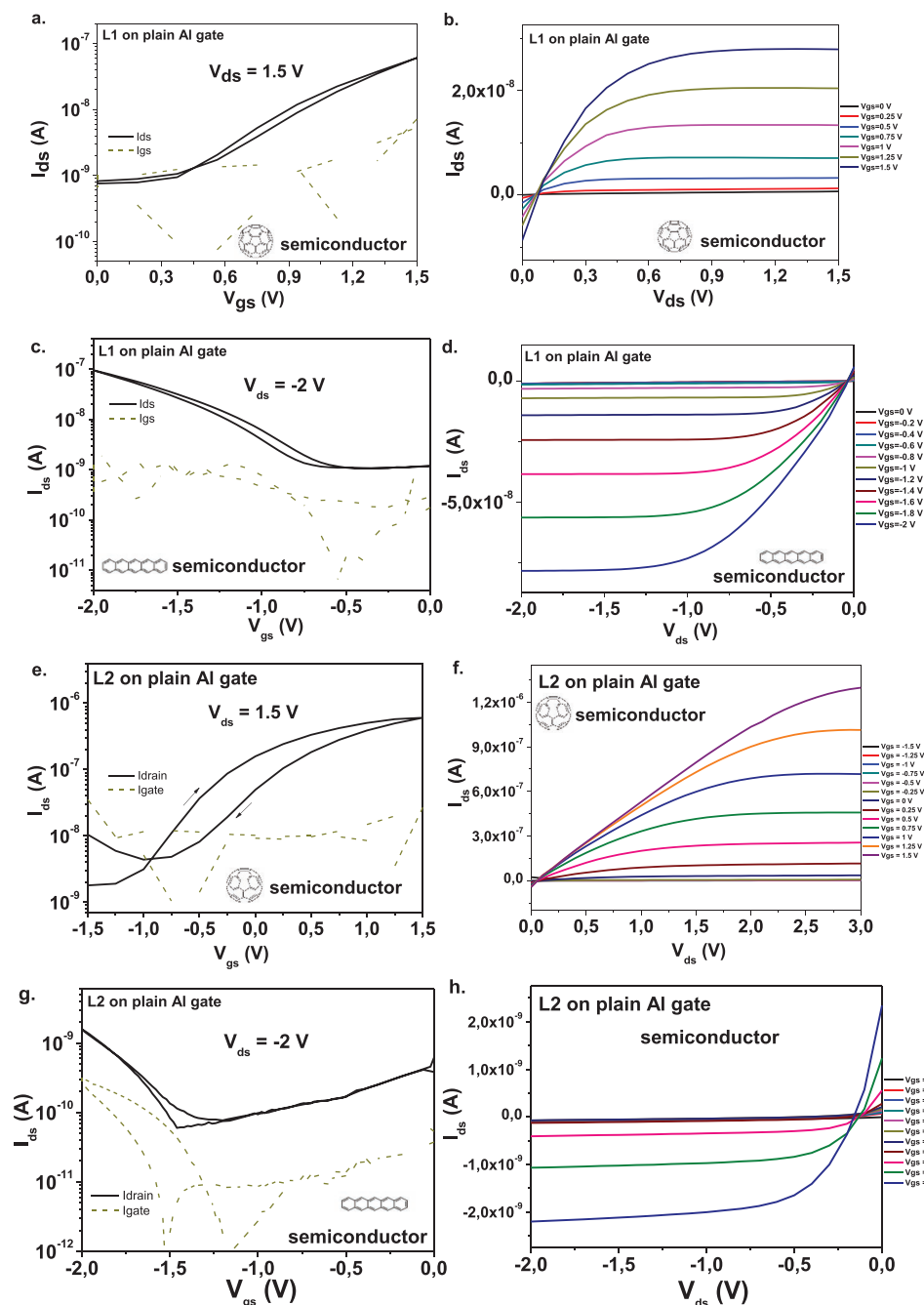


**Figure 10.** Transfer and output characteristic of doctor bladed L1 and L2 lignins on plain aluminum gate, without alumina dielectric: a,b) L1 stand-alone dielectric and fullerene,  $C_{60}$  semiconductor. Specific capacitance  $384.6 \text{ nF cm}^{-2}$ , field effect mobility  $5 \times 10^{-3} \text{ cm}^2 \text{ V}^{-1} \text{ s}^{-1}$ . c,d) L1 stand-alone dielectric and pentacene semiconductor. Specific capacitance  $384.6 \text{ nF cm}^{-2}$ , field effect mobility  $4 \times 10^{-3} \text{ cm}^2 \text{ V}^{-1} \text{ s}^{-1}$ . e,f) L2 stand-alone dielectric and fullerene,  $C_{60}$  semiconductor. Specific capacitance  $238.4 \text{ nF cm}^{-2}$ , field effect mobility  $1.5 \times 10^{-2} \text{ cm}^2 \text{ V}^{-1} \text{ s}^{-1}$ . g,h) L2 stand-alone dielectric and pentacene semiconductor. Specific capacitance  $238.4 \text{ nF cm}^{-2}$ , field effect mobility  $3.2 \times 10^{-4} \text{ cm}^2 \text{ V}^{-1} \text{ s}^{-1}$ .

operating voltage OFET devices. Although the OFET devices presented in this study are not hysteresis free as in the case of other high purity dielectrics investigated by us,<sup>[61,65–69]</sup> we consider that this formulation of lignin is more suitable for future developments of electronic devices through solution processable methods and for the establishment of low-cost fabrication routes for electronics.

In conclusion, our results set the bases for suitable renewable and cost-effective lignin materials deposited through solution methods for electronic devices fabrication. Lignin is by volume the second largest biopolymer on Earth after cellulose, but differently from the latter, it has no real industrial relevance, other than to become the source of valuable chemicals through tedious fractionation processes, or be burned in

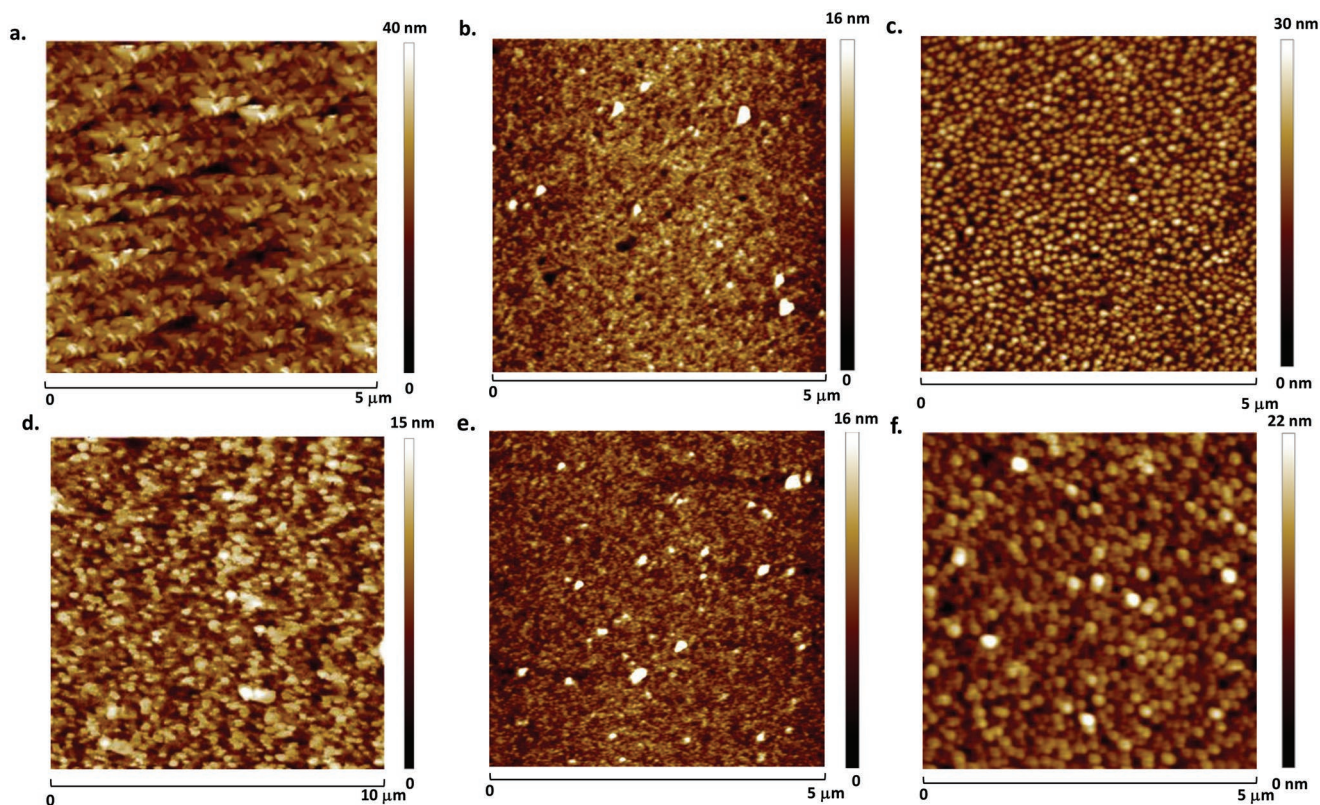


**Figure 11.** AFM pictograms of a) doctor bladed L1 lignin, rms  $\approx$  5.4 nm, b) vacuum processed C<sub>60</sub> on L1 lignin, rms  $\approx$  2.3 nm, c) vacuum processed pentacene on L1 lignin, rms  $\approx$  4.5 nm, d) doctor bladed L2 lignin, rms  $\approx$  2.8 nm, e) C<sub>60</sub> on L2 lignin, rms  $\approx$  2.4 nm, and f) pentacene on L2 lignin, rms  $\approx$  3.0 nm.

order to produce heat and power for the processing plant and potentially for surrounding homes and businesses.<sup>[10,13,70]</sup> We demonstrated through this work that application of commercial lignin in the fabrication of electronic components is a viable avenue to follow in order to reach sustainability for the electronic field by accessing a cheap product of large availability.

#### 4. Experimental Section

**Materials:** The lignin used in this study was purchased from Sigma-Aldrich. L1 is product no. 370 959, while L2 is the product no. 471 003, both obtained in the kraft process, as declared by Sigma-Aldrich. The two lignins were used as received. Cholesterol, 2-chloro-4,4,5,5-tetramethyl-1,3,2-dioxaphospholane (TMDP), chromium (III) acetylacetonate, anhydrous absolute ethanol (EtOH) ammonium hydroxide solution 30% (NH<sub>3</sub> 30% solution), chloroform (CHCl<sub>3</sub>), anhydrous pyridine, and DMSO were purchased from Sigma-Aldrich. Ammonium hydroxide solution (NH<sub>3</sub> 10% solution) was obtained by dilution of commercial ammonium hydroxide solution 30% with deionized water. DMSO-*d*<sub>6</sub> and CDCl<sub>3</sub> for NMR spectra with 99.9 at% D enrichment were purchased from Acros Organics.

**Ash Content:** The ash content was determined with a muffle furnace at 525 °C over 5 h. For L2 lignin, because of the high ash content initially measured, the furnace was kept at 600 °C over 7 h and the procedure was repeated until a constant mass of ash was achieved (after four cycles). All the determinations were done in duplicate.

**Elemental Analysis:** Elemental analyses were performed on an Elementar Vario Micro Cube analyzer. Carbon, hydrogen, nitrogen, and

sulfur contents were determined for the commercial L1 and L2 lignin, and the respective acetylated samples. All analyses were carried out on 5 mg samples to evidence well changes in sulfur or nitrogen content. Oxygen content was calculated for all samples by the difference after ash correction and it was also determined directly. All determinations were done in duplicate.

**FE-SEM/EDS Analysis:** Energy-dispersive X-ray spectroscopy EDS analysis of L2 ashes was performed on an FEI FEG-Quanta 450 instrument (Field Electron and Ion Company, Hillsboro, OR, USA). A Bruker's QUANTAX EBSD/EDS analysis system was used for phase identification and textural mapping. EDS provided basic major element chemistry.

**UV-vis Absorption Spectroscopy:** UV-vis absorption measurements were performed on 0.5 mg mL<sup>-1</sup> solutions of lignin in DMSO at room temperature using a JASCO V-750 spectrophotometer and 0.1 cm path quartz cuvettes.

**ATR-FTIR Spectroscopy:** ATR-FTIR spectra were collected with a Thermo Fischer Nicolet iS50 FTIR instrument interfaced with an ATR ITX accessory equipped with a diamond crystal (radiation penetration  $\approx$  2  $\mu$ m at 1000 cm<sup>-1</sup>). The spectra were recorded at room temperature in the air in the range between 4000 and 650 cm<sup>-1</sup> with a resolution of 4 cm<sup>-1</sup>, 16 accumulated scans, and a DTGS as a detector. The spectra were elaborated using OMNIC software.

**Gel Permeation Chromatography:** Gel permeation chromatography (GPC) analysis was carried out at room temperature using a Malvern Viscotek TDA 305 equipped with a Tosoh Bioscience TSK gel G3000HHR column (7.8 mm i.d. x 30.0 cm l) using a refractive-index detector with chloroform as solvent. Calibration was performed using polystyrene standards. The acylated lignin samples were dissolved in chloroform at 1 mg mL<sup>-1</sup> concentration and filtered prior to the measurement with 0.22  $\mu$ m poly(tetrafluoroethylene) filters.



**EGA-MS:** For the EGA-MS analysis, a Multishot Pyrolyzer EGA/Py-3030D (Frontier Lab, Japan) apparatus was used coupled with a 6890 Agilent Technologies GC and a 5973 Agilent MS Detector operating in electron impact mode at 70 eV. The gas chromatography (GC) oven was equipped with a deactivated and uncoated stainless steel capillary tube (UADTM-2.5 N, 0.15 mm i.d. × 2.5 m length, Frontier Laboratories Ltd.). The sample (about 200 µg) underwent a thermal decomposition in an inert atmosphere over the chosen heating range and evolved gaseous compounds were directly ionized and analyzed as a function of time. Temperature program and other instrumental conditions were the same as ref. [45].

**<sup>31</sup>P-NMR Spectroscopy:** Phosphitylation of lignin samples was performed applying the method described by Crestini et al.<sup>[71]</sup> **L1** and **L2** were dried overnight in an oven set at 40 °C and then transferred in a desiccator until they reached room temperature. A mixture of pyridine and CDCl<sub>3</sub> (1.6:1 v:v ratio) was prepared and dried over molecular sieves. Using this mixture, a 0.1 M solution of the relaxation reagent, chromium (III) acetylacetonate (5 mg mL<sup>-1</sup>), and of internal standard, cholesterol (40 mg mL<sup>-1</sup>), was prepared. All solutions were stored in the dark. Thirty milligrams of **L1** were dissolved in 0.5 mL of solvent solution in a vial equipped with a stirring bar. Thirty milligrams of **L2** were dissolved in 0.3 mL of N,N-dimethylformamide (DMF) and 0.2 mL of solvent solution. Then, 0.1 mL of the internal standard and relaxation solution were added. Complete **L2** solubilization was achieved after 12 h. 0.1 mL of TMDP was added to clear solutions and kept under vigorous magnetic stirring for 30 min. The resulting solution was transferred into an NMR tube. <sup>31</sup>P-NMR spectra were recorded on a JEOL YH spectrometer with a probe operating at 202.468 MHz at 25 °C in CDCl<sub>3</sub>. Chemical shifts were calibrated from the <sup>31</sup>P NMR signal at 132.2 ppm arising from the reaction product between residual water and TMDP. Spectra were quantitative and proton broadband decoupling was applied during the acquisition time. Cholesterol was used as an internal standard. Spectra were acquired with 100 ppm spectral width, 32 000 data points, 15 s relaxation delay, and 128 scans. The spectra were analyzed using JEOL Delta software.

**<sup>13</sup>C-NMR Spectroscopy:** <sup>13</sup>C-NMR was performed on acetylate samples. The acetylation procedure was based on the modified Manson's method.<sup>[71]</sup> The reaction was performed with a 2:1 weight ratio of acetic anhydride to lignin and 1-methylimidazole as a catalyst (0.05 mL g<sup>-1</sup> of lignin) at 55 °C under a nitrogen atmosphere and vigorous stirring overnight. The mixture was quenched with ethyl acetate and washed five times with brine. Acetylated lignin samples were recovered by precipitation with cyclohexane, filtration analyzed drying in vacuo for 8 h. ATR-FTIR analysis was used to check the success of the acetylation reaction. <sup>13</sup>C NMR analyses were performed dissolving 150 mg of samples in 1 mL of DMSO-d<sub>6</sub>. The solutions were clear, and no insoluble fractions were detected. Experiments were carried out on a JEOL YH spectrometer with a probe operating at 100 or 125 MHz and conducted at 50 °C. Chemical shifts are given relative to tetramethylsilane and the position of peaks was referenced to the residual solvent peak of DMSO-d<sub>6</sub> (δ = 39.5 ppm). The spectra were quantitative and acquired with 23 kHz (228 ppm) spectral width, 32 000 data points, an 11 s relaxation delay for a 75° pulse, zero-filling, and 10 Hz line broadening. The spectra were analyzed using JEOL Delta software.

**Organic Semiconductors Purification:** Pentacene and fullerene (C<sub>60</sub>) were purchased from Sigma-Aldrich and purified as reported in ref. [60] by three consecutive train sublimation methods using a quartz tube in vacuum, at a pressure of ≈3 × 10<sup>-6</sup> mbar. Sublimation parameters were: 48 h, 260 °C for pentacene and 380 °C for fullerene.

**OFET Fabrication and Characterization and MIM Measurements:** OFETs were fabricated in bottom-gate top-contact geometry. The staggered structure comprised the gate electrode with either a single layer lignin as dielectric (i.e., **L1** or **L2**) or a dielectric consisting of a combined inorganic (Al<sub>2</sub>O<sub>3</sub>) and organic (lignin, **L1** or **L2**) layer, the organic semiconductor and source and drain electrodes. The alumina layer was grown electrochemically, through a method described elsewhere.<sup>[70,73]</sup> The anodization voltage was set to 10 V and the current compliance to 10 mA. The layer of inorganic dielectric grown electrochemically was ≈17.5 nm, including in this parameter the native oxide layer resulted by

spontaneous oxidation of aluminum in air. Lignin solutions (0.1 g mL<sup>-1</sup>) were prepared using ethanol: 10% aqueous ammonia mixtures in a 1:1 volumetric ratio and films were coated by using the doctor blade method at 2.5 mm/sec speed at 50 °C plate temperature. Then, films were dried on a hot plate for 1 h at 110 °C. Dielectric measurements were performed directly on the MIM structure. For extracting the capacitance of the dielectric layer, the MIM structure belonging to the OFET design was used and the capacitance of the OFET at 1 kHz was extracted for the semiconductor mobility calculation. By doing so, unambiguously the right capacitance that was identical to the one of the transistors that were measured on the same slide was used. A measurement in a wide frequency range spanning from 10 kHz to 1 mHz was performed in an MIM structure with plain aluminum as bottom and top contacts, and the respective lignin layer sandwiched in between them, in order to understand the dielectric behavior in alternating current. The two semiconductors were deposited via physical vapor deposition in a Vaksis evaporator. The typical pressure during the deposition was 1 × 10<sup>-6</sup> mbar, and the deposition rate was kept constant during the evaporation at 0.1 Å s<sup>-1</sup>. The final thickness was 50 nm for both semiconductors. Source and drain electrodes (Al for C<sub>60</sub> and Au for pentacene) were deposited in a metal evaporator through physical vapor deposition. The typical thickness of the source and drain electrodes was 80 nm and the rate of deposition was kept constant at 1 Å s<sup>-1</sup>. The geometric factors of the OFET transistors were: width, W, 2 mm; length of the channel, L, 25 µm.

## Supporting Information

Supporting Information is available from the Wiley Online Library or from the author.

## Acknowledgements

This research received financial support from the University of Pisa through the project "BIHO 2021—Bando Incentivi di Ateneo Horizon e Oltre" (D.d. 408, Prot. no. 0030596/2021) and the program "Visiting Fellow." The authors gratefully acknowledge the support and guidance of Prof. N. S. Sariciftci for this collaboration and his valuable discussions. The authors thank CISUP (Center for Instrument Sharing of the University of Pisa) for the access to the ATR-FTIR and FE-SEM facilities.

## Conflict of Interest

The authors declare no conflict of interest.

## Data Availability Statement

Research data are not shared.

## Keywords

lignin, natural materials, organic field-effect transistors

Received: June 23, 2022

Revised: September 14, 2022

Published online:

[1] Monomers, *Monomers, Polym. Compos. Renewable Resour.* (Eds.: M. R. Belgacem, A. Gandini), Elsevier, New York, 2008.

- [2] M. Irimia-Vladu, E. D. Głowacki, G. Voss, S. Bauer, N. S. Sariciftci, *Mater. Today* **2012**, *15*, 340.
- [3] Green Materials for Electronics, Wiley-VCH Verlag GmbH & Co. KGaA, Weinheim, **2018**.
- [4] H. Erdtman, *J. Polym. Sci. B* **1972**, *10*, 228.
- [5] A. Sakakibara, *Wood Sci. Technol.* **1980**, *14*, 89.
- [6] R. Whetten, R. Sederoff, *Plant Cell* **1995**, *7*, 1001.
- [7] S. Sharma, A. Sharma, S. I. Mulla, D. Pant, T. Sharma, A. Kumar, in *Lignin: Biosynthesis and Transformation for Industrial Applications* (Eds: S. Sharma, A. Kumar), Springer International Publishing, Cham **2020**, pp. 1–15.
- [8] C. J. Biermann, *Handbook of Pulp and Papermaking*, 2nd ed., Academic Press, San Diego, CA **1996**.
- [9] J. S. Luterbacher, D. M. Alonso, J. A. Dumesic, *Green Chem.* **2014**, *16*, 4816.
- [10] D. Stewart, *Ind. Crops Prod.* **2008**, *27*, 202.
- [11] B. M. Upton, A. M. Kasko, *Chem. Rev.* **2016**, *116*, 2275.
- [12] A. Moreno, M. H. Sipponen, *Mater. Horiz.* **2020**, *7*, 2237.
- [13] C. Xu, R. A. D. Arancon, J. Labidi, R. Luque, *Chem. Soc. Rev.* **2014**, *43*, 7485.
- [14] Z. Ding, F. Li, J. Wen, X. Wang, R. Sun, *Green Chem.* **2018**, *20*, 1383.
- [15] S. Wang, M. T. Innocent, Q. Wang, H. Xiang, J. Tang, M. Zhu, *Int. J. Biol. Macromol.* **2020**, *151*, 730.
- [16] B. Wang, T. Shi, Y. Zhang, C. Chen, Q. Li, Y. Fan, *J. Mater. Chem. C* **2018**, *6*, 6423.
- [17] H.-Y. Tse, S.-C. Cheng, C. S. Yeung, C.-Y. Lau, W.-H. Wong, C. Dong, S.-Y. Leu, *Green Chem.* **2019**, *21*, 1319.
- [18] M. H. Sipponen, H. Lange, C. Crestini, A. Henn, M. Österberg, *ChemSusChem* **2019**, *12*, 2039.
- [19] M. Österberg, M. H. Sipponen, B. D. Mattos, O. J. Rojas, *Green Chem.* **2020**, *22*, 2712.
- [20] C. Jin, W. Song, T. Liu, J. Xin, W. C. Hiscox, J. Zhang, G. Liu, Z. Kong, *ACS Sustainable Chem. Eng.* **2018**, *6*, 1763.
- [21] Y. Qian, Q. Zhang, X. Qiu, S. Zhu, *Green Chem.* **2014**, *16*, 4963.
- [22] M. S. Alqahtani, A. Alqahtani, A. Al-Thabit, M. Roni, R. Syed, *J. Mater. Chem. B* **2019**, *7*, 4461.
- [23] W. E. Tenhaeff, O. Rios, K. More, M. A. McGuire, *Adv. Funct. Mater.* **2014**, *24*, 86.
- [24] N. Hong, J. Xiao, Y. Li, Y. Li, Y. Wu, W. Yu, X. Qiu, R. Chen, H.-L. Yip, W. Huang, Y. Cao, *J. Mater. Chem. C* **2016**, *4*, 5297.
- [25] Y. Zhao, Y. Liu, C. Tong, J. Ru, B. Geng, Z. Ma, H. Liu, L. Wang, *J. Mater. Sci.* **2018**, *53*, 7637.
- [26] L. Liu, N. Solin, O. Inganäs, *Adv. Energy Mater.* **2021**, *11*, 2003713.
- [27] J. C. de Haro, E. Tatsi, L. Fagiolari, M. Bonomo, C. Barolo, S. Turri, F. Bella, G. Griffini, *ACS Sustainable Chem. Eng.* **2021**, *9*, 8550.
- [28] Y. Xu, K. Odelius, M. Hakkarainen, *ACS Sustainable Chem. Eng.* **2019**, *7*, 13456.
- [29] S. Zhang, T. Liu, C. Hao, L. Wang, J. Han, H. Liu, J. Zhang, *Green Chem.* **2018**, *20*, 2995.
- [30] J. Huang, W. Liu, X. Qiu, *ACS Sustainable Chem. Eng.* **2019**, *7*, 6550.
- [31] M. Oliviero, R. Rizvi, L. Verdolotti, S. Iannace, H. E. Naguib, E. Di Maio, H. C. Neitzert, G. Landi, *Adv. Funct. Mater.* **2017**, *27*, 1605142.
- [32] Q. Fan, T. Liu, C. Zhang, Z. Liu, W. Zheng, R. Ou, Q. Wang, *J. Mater. Chem. A* **2019**, *7*, 23162.
- [33] M. Borrega, S. Päärnilä, L. G. Greca, A.-S. Jääskeläinen, T. Ohra-aho, O. J. Rojas, T. Tamminen, *Langmuir* **2020**, *36*, 9675.
- [34] M. Irimia-Vladu, E. D. Głowacki, G. Schwabegger, L. Leonat, H. Z. Akpinar, H. Sitter, S. Bauer, N. S. Sariciftci, *Green Chem.* **2013**, *15*, 1473.
- [35] M. Irimia-Vladu, Y. Kanbur, F. Camaioni, M. E. Coppola, C. Yumusak, C. V. Irimia, A. Vlad, A. Operamolla, G. M. Farinola, G. P. Suranna, N. González-Benitez, M. C. Molina, L. F. Bautista, H. Langhals, B. Stadlober, E. D. Głowacki, N. S. Sariciftci, *Chem. Mater.* **2019**, *31*, 6315.
- [36] E. D. Głowacki, R. R. Tangorra, H. Coskun, D. Farka, A. Operamolla, Y. Kanbur, F. Milano, L. Giotta, G. M. Farinola, N. S. Sariciftci, *J. Mater. Chem. C* **2015**, *3*, 6554.
- [37] A. Operamolla, S. Casalini, D. Console, L. Capodiecchi, F. Di Benedetto, G. V. Bianco, F. Babudri, *Soft Matter* **2018**, *14*, 7390.
- [38] S. Sawalha, F. Milano, M. R. Guascito, S. Bettini, L. Giotta, A. Operamolla, T. Da Ros, M. Prato, L. Valli, *Carbon* **2020**, *167*, 906.
- [39] J. Ko, W. L. Leong, *2020 4th IEEE Electron Devices Technology and Manufacturing Conference (EDTM) 2020*, pp. 1–3.
- [40] N.-E. E. Mansouri, J. Salvadó, *Ind. Crops Prod.* **2006**, *24*, 8.
- [41] G. Gellerstedt, *Ind. Crops Prod.* **2015**, *77*, 845.
- [42] U. P. Agarwal, R. H. Atalla, in *Lignins and Lignans: Advances in Chemistry*, CRC Press, Boca Raton **2010**.
- [43] C.-S. Wu, *Polym. Degrad. Stab.* **2009**, *94*, 1076.
- [44] K. Wang, F. Xu, R. Sun, *Int. J. Mol. Sci.* **2010**, *11*, 2988.
- [45] A. Gärtner, G. Gellerstedt, T. Tamminen, *Nord. Pulp Pap. Res. J.* **1999**, *14*, 163.
- [46] T. Yamasaki, S. Hosoya, C.-L. Chen, J. S. Gtrazl, H.-M. Chang, in *Proceedings of the International Symposium on Wood and Pulping Chemistry*, Stockholm, Sweden **1981**, 34.
- [47] G. Gellerstedt, E.-L. Lindfors, *Nord. Pulp Pap. Res. J.* **1987**, *2*, 71.
- [48] K. Lundquist, in *Methods in Lignin Chemistry* (Eds: S. Y. Lin, C. W. Dence), Springer, Heidelberg **1992**, p. 242.
- [49] D. Robert, in *Methods in Lignin Chemistry*, (Eds: S. Y. Lin, C. W. Dence), Springer, Heidelberg **1992**, p. 250.
- [50] C. A. Cateto, M. F. Barreiro, A. E. Rodrigues, M. C. Brochier-Salon, W. Thielemans, M. N. Belgacem, *J. Appl. Polym. Sci.* **2008**, *109*, 3008.
- [51] A. Granata, D. S. Argyropoulos, *J. Agric. Food Chem.* **1995**, *43*, 1538.
- [52] X. Meng, C. Crestini, H. Ben, N. Hao, Y. Pu, A. J. Ragauskas, D. S. Argyropoulos, *Nat. Protoc.* **2019**, *14*, 2627.
- [53] C. Zhao, J. Huang, L. Yang, F. Yue, F. Lu, *Ind. Eng. Chem. Res.* **2019**, *58*, 5707.
- [54] D. Tamburini, J. J. Łucejko, E. Ribechini, M. P. Colombini, *J. Mass Spectrom.* **2015**, *50*, 1103.
- [55] D. Tamburini, C. R. Cartwright, P. Gasson, J. J. Łucejko, C. L. D. Leme, *J. Anal. Appl. Pyrolysis* **2020**, *151*, 104909.
- [56] A. Shiono, A. Hosaka, C. Watanabe, N. Teramae, N. Nemoto, H. Ohtani, *Polym. Test.* **2015**, *42*, 54.
- [57] S. Wang, G. Dai, H. Yang, Z. Luo, *Prog. Energy Combust. Sci.* **2017**, *62*, 33.
- [58] J. J. Łucejko, D. Tamburini, F. Modugno, E. Ribechini, M. P. Colombini, *Appl. Sci.* **2021**, *11*, 240.
- [59] M. Egginger, M. Irimia-Vladu, R. Schwödiauer, A. Tanda, I. Frischauf, S. Bauer, N. S. Sariciftci, *Adv. Mater.* **2008**, *20*, 1018.
- [60] C. Yumusak, N. S. Sariciftci, M. Irimia-Vladu, *Mater. Chem. Front.* **2020**, *4*, 3678.
- [61] J. Ivić, A. Petritz, C. V. Irimia, B. Kahraman, Y. Kanbur, M. Bednorz, C. Yumusak, M. A. Aslam, A. Matković, K. Saller, C. Schwarzingler, W. Schühly, A. I. Smeds, Y. Salinas, M. Schiek, F. Mayr, C. Xu, C. Teichert, M. Osiac, N. S. Sariciftci, B. Stadlober, M. Irimia-Vladu, *Adv. Sustainable Syst.* **2022**, 2200234.
- [62] R. D'Orsi, J. J. Łucejko, F. Babudri, A. Operamolla, A. C. S. Omega, **2022**, *7*, 25253.
- [63] S. Steudel, S. De Vusser, S. De Jonge, D. Janssen, S. Verlaak, J. Genoe, P. Heremans, *Appl. Phys. Lett.* **2004**, *85*, 4400.
- [64] I. P. M. Bouchoms, W. A. Schoonveld, J. Vrijmoeth, T. M. Klapwijk, *Synth. Met.* **1999**, *104*, 175.
- [65] M. Irimia-Vladu, N. Marjanovic, M. Bodea, G. Hernandez-Sosa, A. M. Ramil, R. Schwödiauer, S. Bauer, N. S. Sariciftci, F. Nüesch, *Org. Electron.* **2009**, *10*, 408.
- [66] Y. Kanbur, M. Irimia-Vladu, E. D. Głowacki, G. Voss, M. Baumgartner, G. Schwabegger, L. Leonat, M. Ullah, H. Sarica, S. Erten-Ela, R. Schwödiauer, H. Sitter, Z. Küçükyavuz, S. Bauer, N. S. Sariciftci, *Org. Electron.* **2012**, *13*, 919.



- [67] G. Schwabegger, M. Ullah, M. Irimia-Vladu, M. Baumgartner, Y. Kanbur, R. Ahmed, P. Stadler, S. Bauer, N. S. Sariciftci, H. Sitter, *Synth. Met.* **2011**, 161, 2058.
- [68] A. Petritz, A. Wolfberger, A. Fian, T. Griesser, M. Irimia-Vladu, B. Stadlober, *Adv. Mater.* **2015**, 27, 7645.
- [69] M. Baumgartner, M. E. Coppola, N. S. Sariciftci, E. D. Glowacki, S. Bauer, M. Irimia-Vladu, *Green Mater. Electron.* **2017**, 1.
- [70] M. Kaltenbrunner, T. Sekitani, J. Reeder, T. Yokota, K. Kuribara, T. Tokuhara, M. Drack, R. Schwödiauer, I. Graz, S. Bauer-Gogonea, S. Bauer, T. Someya, *Nature* **2013**, 499, 458.
- [71] D. S. Argyropoulos, N. Pajer, C. Crestini, *J. Vis. Exp.* **2021**, 174, e62696.
- [72] W. Thielemans, R. P. Wool, *Biomacromolecules* **2005**, 6, 1895.
- [73] A. I. Mardare, M. Kaltenbrunner, N. S. Sariciftci, S. Bauer, A. W. Hassel, *Phys. Status Solidi A* **2012**, 209, 813.